Inorganic Chemistry

Article

pubs.acs.org/IC

An Octanuclear Molybdenum(VI) Complex Containing Coordinatively Bound 4,4′-di-*tert*-Butyl-2,2′-Bipyridine, $[Mo_8O_{22}(OH)_4(di\text{-}tBu\text{-}bipy)_4]$: Synthesis, Structure, and Catalytic Epoxidation of Bio-Derived Olefins

Tatiana R. Amarante,[†] Patrícia Neves,[†] Cátia Tomé,[‡] Marta Abrantes,[‡] Anabela A. Valente,[†] Filipe A. Almeida Paz,[†] Martyn Pillinger,[†] and Isabel S. Gonçalves*[,†]

[†]Department of Chemistry, CICECO, University of Aveiro, 3810-193 Aveiro, Portugal

[‡]Centro de Química Estrutural, Complexo Interdisciplinar, Instituto Superior Técnico, Universidade Técnica de Lisboa, Av. Rovisco Pais, 1, 1049-001 Lisboa, Portugal

Supporting Information

ABSTRACT: The reaction of $[MoO_2Cl_2(di\text{-}tBu\text{-}bipy)]$ (**1**) (di-*t*Bu-bipy = 4,4′-di-*tert*-butyl-2,2′-bipyridine) with water at 100−120 °C in a Teflon-lined stainless steel autoclave, in an open reflux system, or in a microwave synthesis system gave the octanuclear complex $[Mo_8O_{22}(OH)_4(di\text{-}tBu\text{-}bipy)_4]$ (**2**) as a microcrystalline powder in good yields. Single crystals of **2** suitable for X-ray diffraction were obtained by the reaction of MoO_3 and di-*t*Bu-bipy in water at 160 °C for 3 days. The molecular structure of **2** comprises a purely inorganic core, $Mo_4O_8(\mu_3\text{-}OH)_2(\mu_2\text{-}O)_2$, attached to two peripheral oxo-bridged binuclear units, $Mo_2O_4(\mu_2\text{-}O)_2(OH)(di\text{-}tBu\text{-}bipy)_2$. The inorganic core is composed of a unique assembly of four $\{MoO_5\}$ distorted square pyramids connected to each other *via* edge-sharing. Overall, the octanuclear complex adopts a highly distorted form strongly resembling an "S"-shaped molecular unit. Complex **2** was applied in the catalytic epoxidation of the biorenewable olefins DL-limonene (Lim) and methyl oleate (Ole), using *tert*-butylhydroperoxide (TBHP) as an oxygen donor, under mild reaction conditions (55 °C, air). The reactions of Lim and Ole gave the respective epoxide monomers in fairly high selectivities at high conversions (89% 1,2-epoxy-*p*-menth-8-ene selectivity at 96% Lim conversion; 99% methyl 9,10-epoxystearate selectivity at 94% Ole conversion, reached within 24 h reaction). Iodometric titrations revealed no measurable "non-productive" decomposition of TBHP.

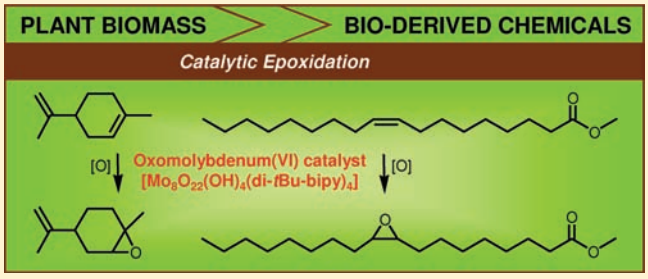

INTRODUCTION

Oxomolybdenum hybrid materials have been of interest for several years due to their potentially interesting catalytic, magnetic, electronic, and optical properties.[1,2] One class of molybdenum oxide composites that has attracted particular interest is that in which the organic component is an organonitrogen compound. Zubieta and co-workers identified three subclasses for these materials based on the role of the organic molecule: (1) a charge-compensating, space-filling, and structure-directing cation, (2) a ligand bonded to a heterometal center which is incorporated into the metal oxide backbone either as peripheral moieties or as complex bridging units, and (3) a ligand bonded directly to a molybdenum site of the oxide substructure.[1] Ligands examined for the latter include 2,2′-bipyridine (2,2′-bipy),[2a−c] 4,4′-bipyridine,[2d−f] 4,4′-bipyridylamine,[2g] 1,10-phenanthroline,[2h] 2-[3(5)-pyrazolyl]pyridine (pzpy),[2i] pyrazine,[2j] 2,4,6-tripyridyltriazine,[2k] 1,2,3-triazole,[2l] and 1,2,4-triazoles.[2m] Owing to the pronounced structure-directing influence of organoamines, the structural chemistry of these materials encompasses one-dimensional (1D) chains, two-dimensional (2D) sheets, and three-dimensional (3D) networks, as well as discrete clusters.

Molybdenum oxide/organoamine hybrids are generally prepared by the hydrothermal treatment at 160−200 °C of aqueous solutions containing the organonitrogen compound and the molybdenum source, which is usually Na_2MoO_4, MoO_3, or $(NH_4)_6Mo_7O_{24}$. This method frequently affords crystals suitable for X-ray diffraction. On the other hand, yields can be low, and mixtures of phases are sometimes obtained that require mechanical separation. We have been exploring alternative approaches that use monomeric molybdenum complexes as precursors. Thus, the oxidative decarbonylation of the tetracarbonyl complexes $[Mo(CO)_4(L)]$ (L = 2,2′-bipy, pzpy) by reaction with *tert*-butylhydroperoxide at room temperature gives microcrystalline $[MoO_3(2,2'\text{-}bipy)]$ and $[Mo_4O_{12}(pzpy)_4]$ in excellent yields.[3,4] In these compounds, $\{MoO_4N_2\}$ octahedra share corners to form 1D chains in the former and tetranuclear square-type species in the latter. For L = 4,4′-di-*tert*-butyl-2,2′-bipyridine (di-*t*Bu-bipy), the octanuclear complex $[Mo_8O_{24}(di\text{-}tBu\text{-}bipy)_4]$ containing a central cubane-type $Mo_4(\mu_3\text{-}O)_4$ core is obtained.[3] The controlled hydrolysis

Received: December 7, 2011
Published: February 28, 2012

dx.doi.org/10.1021/ic202640a | *Inorg. Chem.* 2012, 51, 3666−3676

and condensation of monomeric complexes of the type $[MoO_2Cl_2L]$ is another potentially interesting route to molybdenum oxide/organic hybrids. The reaction of $[MoO_2Cl_2(2,2'\text{-bipy})]$ with water at 100−120 °C gives $\{[MoO_3(2,2'\text{-bipy})][MoO_3(H_2O)]\}_n$ with a crystal structure containing 1D inorganic and organic−inorganic polymers linked by O−H···O hydrogen bonds.[5]

The synthesis of the aforementioned molybdenum oxide/organodiamine compounds in high yields under mild conditions has paved the way to catalytic applications. In preliminary investigations these materials have proved to be active, selective, and stable catalysts for the epoxidation of *cis*-cyclooctene, used as a model substrate.[3−5] Future work will need to address the epoxidation of more demanding olefins and/or other types of oxidation reactions.

As part of our ongoing investigations into the use of molybdenum complexes as precursors to oxomolybdenum hybrids, we now report on results with the complex $[MoO_2Cl_2(\text{di-}t\text{Bu-bipy})]$ (**1**). Several studies in the literature indicate that di-*t*Bu-bipy is a good choice as a ligand for oxometal complexes to be used as catalysts for oxidation reactions.[6] For example, in addition to the octanuclear complex mentioned above,[3] the complexes $[MoO_2(NCS)_2(\text{di-}t\text{Bu-bipy})]$,[6a−d] $[Mo_2O_5(NCS)_2(\text{di-}t\text{Bu-bipy})_2]$,[6d] and $[V_2O_2(\mu\text{-MeO})_2(\mu\text{-MO}_4)_2(\text{di-}t\text{Bu-bipy})_2]$ (M = Mo, W)[6g] are effective as oxygen atom transfer agents and/or (pre)catalysts for alcohol oxidation and olefin epoxidation. Kodama et al. concluded that the affinity of the heterotetranuclear V_2W_2 complex to organic substrates was improved by the selection of di-*t*Bu-bipy as the organic ligand.[6g]

Hydrolysis of **1** using various heating methods gives $[Mo_8O_{22}(OH)_4(\text{di-}t\text{Bu-bipy})_4]$ (**2**) with a structure that comprises a purely inorganic core, $Mo_4O_8(\mu_3\text{-OH})_2(\mu_2\text{-O})_2$, attached to two peripheral oxo-bridged binuclear units, $Mo_2O_4(\mu_2\text{-O})_2(OH)(\text{di-}t\text{Bu-bipy})_2$. Octanuclear **2** can also be obtained by the hydrothermal treatment of an aqueous solution containing MoO_3 and di-*t*Bu-bipy. Complex **2** was applied in the catalytic epoxidation of *R*-(+)-limonene and methyl oleate, which were chosen as substrates due to their relevance to the use of plant biomass as a renewable feedstock for the chemical industry.[7]

EXPERIMENTAL SECTION

Materials and Methods. The monomer $[MoO_2Cl_2(\text{di-}t\text{Bu-bipy})]$ (**1**) was synthesized according to the published procedure.[8] MoO_3 (99.5%, AnalaR), MoO_2Cl_2 (Sigma-Aldrich), 4,4′-di-*tert*-butyl-2,2′-bipyridine (Sigma-Aldrich), diethyl ether (Sigma-Aldrich, puris, p.a.), acetone (Fluka, puris, p.a.), toluene (Riedel-de-Haën, puris, p.a.), and dichloromethane (Fluka, puris, p.a.) were obtained from commercial sources and used as received. Microanalyses (CHN) were provided by the Mass Spectrometry Laboratory, New University of Lisbon. FT-IR spectra were recorded as KBr pellets using a Unicam-Mattson 7000 spectrophotometer equipped with a DTGS CsI detector. Attenuated total reflectance (ATR) spectra were measured on the same instrument equipped with a Specac Golden Gate Mk II ATR accessory having a diamond top-plate and KRS-5 focusing lenses. FT-Raman spectra were recorded on a RFS-100 Bruker FT-Spectrometer equipped with a Nd:YAG laser with an excitation wavelength of 1064 nm and a laser power set to 94 mW. ^{13}C cross-polarization (CP) magic-angle-spinning (MAS) NMR spectra were obtained using a Bruker Avance 400 spectrometer (9.4 T) at 100.62 MHz, with 3.6 μs ^1H 90° pulses, 2 ms contact time, spinning rates of 7 and 11 kHz, and 5 s recycle delays. Chemical shifts are quoted in parts per million (ppm) with respect to TMS. ^1H NMR spectra in solution were recorded on a Bruker Avance II+ 400 MHz (UltraShieldTM Magnet) spectrometer at ambient temperature. Powder X-ray diffraction (PXRD) data for all synthesized materials were collected at ambient temperature on an X'Pert MPD Philips diffractometer, equipped with an X'Celerator detector and a flat-plate sample holder in a Bragg−Brentano para-focusing optics configuration (40 kV, 50 mA). Intensity data were collected by the step-counting method (step 0.04°), in continuous mode, in the ca. $3.5 \leq 2\theta \leq 70°$ range. The microwave-assisted syntheses were carried out in a Discover S-Class (CEM Corporation, USA) microwave oven using a glass vessel with a capacity of 35 mL. A dynamic method was used in which the power was automatically controlled on the basis of the temperature feedback measured using a vertical focused IR sensor.

$[Mo_8O_{22}(OH)_4(\text{di-}t\text{Bu-bipy})_4]$ (2). *Method A.* A mixture of **1** (0.25 g, 0.53 mmol) and water (25 mL) was stirred and heated to 120 °C inside a microwave oven and maintained at this temperature for 4.5 h. The resultant white solid was separated from the pink aqueous mother liquor (pH ≅ 2) by filtration; washed with water, acetone/diethyl ether (1:1), and diethyl ether (10 mL each); and finally vacuum-dried. Yield: 0.092 g, 61% (based on Mo). Anal. Calcd for $C_{72}H_{100}Mo_8N_8O_{26}$ (2261.12): C, 38.24; H, 4.45; N, 4.95. Found: C, 37.80; H, 4.31; N, 4.94. Selected FT-IR (cm^{-1}): ν = 3262 (m), 2967 (s), 2936 (sh), 2906 (m), 2870 (m), [1615 (vs), 1548 (m), 1410 (vs) (bipy C═C and C═N str)], [935 (vs), 923 (s), 914 (vs), 899 (vs), 882 (vs), 865 (vs) ν(Mo═O)], 850 (vs) (ligand mode), [829 (vs), 777 (vs), 751 (s), 719 (s), 640 (vs,br) ν(Mo−O−Mo) and $\nu(OMo_3)$]. Selected FT-Raman (cm^{-1}): ν = 3072 (m), 2972 (s), 2929 (m), 2905 (m), 1608 (s), 1541 (vs), 1415 (s), 1318 (vs), 957 (s), 934 (vs), 922 (vs), 900 (s), 863 (s), 827 (m), 802 (m), 781 (m), 718 (s). ^1H NMR (400 MHz, CD_3CN, 25 °C, ppm): δ = 8.56 (d, bipy), 8.44 (s, bipy), 7.43 (d, bipy), 1.37 (s, $C(CH_3)_3$). ^{13}C CP MAS NMR: δ = 31.0, 31.6 ($(CH_3)_3C$, $(CH_3)_3C'$), 34.9, 36.0 ($(CH_3)_3C$, $(CH_3)_3C'$), 117.3−120.0, 126.3, 150.1, 151.1, 151.9, 153.4, 162.7, 163.9, 167.3 (C(2,2′)-C(6,6′)).

Method B. A Schlenk tube was charged with **1** (0.97 g, 2.08 mmol) and water (60 mL), and the mixture was refluxed for 18 h under air using an external oil bath as a heating source. The resultant white solid was separated from the pink aqueous mother liquor (pH ≅ 2) by filtration; washed with water, *n*-hexane, and diethyl ether (10 mL each); vacuum-dried; and identified as **2** (0.42 g, 72%; based on Mo) by elemental analysis, FT-IR spectroscopy, and PXRD.

Method C. A Teflon-lined stainless steel autoclave was charged with **1** (0.16 g, 0.34 mmol) and water (10 mL) and heated in an oven at 100 °C for 19 h. The resultant white solid was separated from the pink aqueous mother liquor (pH ≅ 2) by filtration; washed with water, *n*-hexane, and diethyl ether (10 mL each); vacuum-dried; and identified as **2** (0.065 g, 68%; based on Mo) by elemental analysis, FT-IR spectroscopy, and PXRD.

Method D. A Teflon-lined stainless steel autoclave was charged with MoO_3 (0.34 g, 2.4 mmol), di-*t*Bu-bipy (0.64 g, 2.4 mmol), and water (25 mL) and heated in an oven at 160 °C for 3 days with rotation at 25 rpm. A light pink solid and small single crystals suspended in a colorless solution (pH ≅ 5) were obtained. Crystals were directly harvested from the reaction vessel and immediately immersed in highly viscous FOMBLIN Y perfluoropolyether vacuum oil (LVAC 140/13) for X-ray diffraction analysis. The remaining solid material was isolated by filtration; washed with water, *n*-hexane, and diethyl ether (10 mL each); vacuum-dried; and identified as **2** (0.47 g, 70%; based on Mo) by elemental analysis, FT-IR spectroscopy, and PXRD.

Single Crystal X-Ray Diffraction. A single-crystal of $[Mo_8O_{22}(OH)_4(\text{di-}t\text{Bu-bipy})_4]$ (**2**) was mounted on a very thin Hampton Research CryoLoop[9] with the help of a Stemi 2000 stereomicroscope equipped with Carl Zeiss lenses. Data were collected at 150(2) K on a Bruker X8 Kappa APEX II CCD area-detector diffractometer (Mo Kα graphite-monochromated radiation, λ = 0.71073 Å) controlled by the APEX2 software package[10] and equipped with an Oxford Cryosystems Series 700 cryostream monitored remotely using Cryopad.[11] Because of the very small dimensions of the available crystals (maximum dimension of *ca.* 0.01 mm—the real

dx.doi.org/10.1021/ic202640a | *Inorg. Chem.* 2012, 51, 3666−3676

crystal dimensions could be smaller), in conjunction with the low crystal symmetry and relatively large unit cell, diffraction at high angles was very poor. The collected data set was ultimately composed of frames integrated over a period of 300 s and with 1° per frame. Images were processed using SAINT+,[12] and data were corrected for absorption by the multiscan semiempirical method implemented in SADABS.[13] Due to poor diffraction, the mean I/σ values were only over unity for resolutions lower than 1.05 Å, hence the very high R_{int} value for the employed data set (Table 1). The overall quality of the data set may only be improved by using either a synchrotron or a rotating anode source.

Table 1. Crystal and Structure Refinement Data for $[Mo_8O_{22}(OH)_4(di\text{-}tBu\text{-}bipy)_4]$ (2)

formula	$C_{72}H_{100}Mo_8N_8O_{26}$
fw	2261.12
cryst syst	triclinic
space group	$P\bar{1}$
a (Å)	12.90(2)
b (Å)	13.111(18)
c (Å)	13.46(2)
α [deg]	65.98(4)
β [deg]	85.61(5)
γ [deg]	84.51(5)
V [Å^3]	2068(5)
Z	1
D_{calcd} [g cm^{-3}]	1.815
μ(Mo Kα) [mm^{-1}]	1.252
cryst size [mm]	0.01 × 0.01 × 0.01
cryst type	colorless block
θ range [deg]	3.52 to 25.35
index ranges	$-15 \le h \le 15$, $-15 \le k \le 15$, $-16 \le l \le 15$
reflns collected	21721
independent reflns	7211 [R_{int} = 0.3014]
completeness to θ = 25.35°	95.2%
final R indices [$I > 2\sigma(I)$][a,b]	R1 = 0.0995, wR2 = 0.2051
final R indices (all data)[a,b]	R1 = 0.3317, wR2 = 0.3114
weighting scheme[c]	m = 0.1181, n = 0.0
largest diff. peak and hole	1.500 and −1.676 eÅ^{-3}

[a] $R1 = \sum||F_o| - |F_c||/\sum|F_o|$. [b] $wR2 = (\sum[w(F_o^2 - F_c^2)^2]/\sum[w(F_o^2)^2])^{1/2}$. [c] $w = 1/[\sigma^2(F_o^2) + (mP)^2 + nP]$ where $P = (F_o^2 + 2F_c^2)/3$.

The crystal structure was solved using the Patterson synthesis algorithm implemented in SHELXS-97,[14] which allowed the immediate location of the four crystallographically independent molybdenum centers. All remaining non-hydrogen atoms were located from difference Fourier maps calculated from successive full-matrix least-squares refinement cycles on F^2 using SHELXL-97.[14a,15] Non-hydrogen atoms composing the $[Mo_8O_{22}(OH)_4(di\text{-}tBu\text{-}bipy)_4]$ molecular unit were successfully refined using anisotropic displacement parameters.

The oxidation states of the molybdenum centers were unequivocally confirmed by using bond valence calculations following the theoretical models of Brese and O'Keeffe[16] and of Brown and Altermatt[17] and based on the measured Mo−O and Mo−N interactions. Calculations were performed using PLATON.[18] The sums of the bond valences at each metal atomic position are as follows (considering a +6 oxidation state for each metal center): Mo1 +5.92, Mo2 +5.80, Mo3 +6.19, and Mo4 +6.16. These results clearly suggest that the oxidation states of the four crystallographically independent metal centers are +6. This structural evidence supports the existence of four hydroxyl groups (as ultimately modeled into the crystal structure) and is well in line with the results previously described by us for the related octanuclear $[Mo_8O_{24}(di\text{-}tBu\text{-}bipy)_4]$ windmill-type complex.[3]

Hydrogen atoms bound to carbon were placed at their idealized positions using appropriate *HFIX* instructions in SHELXL: *43* for the aromatic and *137* for the terminal $-CH_3$ methyl groups belonging to the di-*t*Bu-bipy ligands. All of these atoms were included in subsequent refinement cycles in riding-motion approximation with isotropic thermal displacement parameters (U_{iso}) fixed at 1.2 or 1.5 × U_{eq} of the respective parent carbon atom (for CH (aromatic) and CH_3, respectively). The overall quality of the collected data set did not allow the hydrogen atoms associated with the terminal (O13) and μ_3-bridging (O1) oxygen atoms to be sensibly located from difference Fourier maps, and so these were also placed in calculated positions using *HFIX 147* and *13* instructions, respectively, in SHELXL and were refined with U_{iso} = 1.5 × U_{eq} of the parent oxygen atom.

The last difference Fourier map synthesis showed the highest peak (1.500 eÅ^{-3}) and deepest hole (−1.676 eÅ^{-3}) located at 1.20 Å and 0.96 Å from Mo1, respectively. Information concerning crystallographic data collection and structure refinement details is summarized in Table 1. CCDC-856220 contains the supplementary crystallographic data for this paper (including structure factors). These data can be obtained free of charge from The Cambridge Crystallographic Data Centre via www.ccdc.cam.ac.uk/data_request/cif.

Catalysis. The catalytic epoxidation reactions were carried out in 5 mL borosilicate reactors immersed in a thermostatted oil bath at 55 °C, under magnetic stirring (800 rpm) and autogenous pressure. The reagents were separately preheated to 55 °C prior to initializing the catalytic reaction by adding the oxidant to the reactor containing the olefin/catalyst. The solvents were distilled, and solvents and reagents were predried using activated 3 or 4 Å molecular sieves. Typically, the initial molar ratio of molybdenum/olefin/oxidant was 1:100:152 (18 μmol Mo). When 5.5 M *tert*-butylhydroperoxide in decane was the oxidant solution used, the reactions were performed either without additional solvent (TBHPdec) or with 1 mL of 1,2-dichloroethane (DCE), acetonitrile, ethyl acetate (EtOAc), ethanol (EtOH), or benzotrifluoride (BTF) as a cosolvent (TBHPdec/cosolvent). Mixtures denoted as TBHP/DCE and TBHP/EtOH were prepared by mixing 70% aqueous TBHP and a solvent and subsequently eliminating the excess water using magnesium sulfate. TBHP concentrations of these TBHP/cosolvent mixtures were determined by iodometric titrations. After each 24 h batch run, the solid phase was separated from the liquid phase by centrifugation, thoroughly washed with hexane, dried at room temperature overnight, and characterized by ATR FT-IR spectroscopy. The evolutions of the catalytic reactions were monitored by using a Varian 3900 GC equipped with a flame ionization detector and a DB-5 capillary column (30 m × 0.25 mm × 0.25 μm); undecane and methyl decanoate were used as internal standards for the reactions of DL-limonene and methyl oleate, respectively. The reaction products were identified by GC-MS (Trace GC 2000 Series Thermo Quest CE Instruments GC; Thermo Scientific DSQ II) using He as the carrier gas.

RESULTS AND DISCUSSION

Synthesis of $[Mo_8O_{22}(OH)_4(di\text{-}tBu\text{-}bipy)_4]$ (2). The reaction of $[MoO_2Cl_2(di\text{-}tBu\text{-}bipy)]$ (**1**) with water was carried out either in a sealed glass vessel with microwave-assisted heating (120 °C, 4.5 h, method A), in an open reflux system in the air (18 h, oil bath heating, method B), or in a sealed Teflon-lined stainless steel digestion bomb (autogenous pressure, 100 °C, 19 h, method C). In each case, a white solid suspended in an acidic solution (pH ≅ 2) was obtained, which was recovered by filtration, washed with water and organic solvents, and vacuum-dried. Practically identical elemental analysis, FT-IR, and PXRD data were obtained for all three solid products, indicating that the heating method had no significant influence on the outcome of the reaction (Figures S1 and S2 in the Supporting Information). The same product could be synthesized from MoO_3, di-*t*Bu-bipy, and H_2O in the molar ratio 1:1:580 at 160 °C for 3 days in a Teflon-lined digestion bomb rotating at 25 rpm. In addition to microcrystalline

dx.doi.org/10.1021/ic202640a | Inorg. Chem. 2012, 51, 3666−3676

material, this reaction gave very small single crystals (maximum dimension of *ca.* 0.01 mm), which were subjected to X-ray diffraction analyses (described below).[19] When the latter reaction was carried out without rotation, the main product was contaminated with unreacted MoO_3. Performing the reaction of MoO_3 with di-*t*Bu-bipy under conditions equivalent to those used in methods A and B gave either a mixture of unreacted MoO_3 + compound **2** (method A) or a mixture of compound **2** and the dinuclear complex $[\{MoO_2(\mu\text{-}O)(\text{di-}t\text{Bu-bipy})\}_2]$ (method B).[19]

On the basis of the characterization data and the crystal structure solution described below, the product from methods A–D is formulated as $[Mo_8O_{22}(OH)_4(\text{di-}t\text{Bu-bipy})_4]$ (**2**) (Scheme 1). Yields were 61% for method A and 70 ± 2% for methods B–D. The microcrystalline powders were phase-pure and the PXRD patterns were in agreement with a simulated pattern calculated from the crystal structure data for **2** (Figure S2). The formula for **2** implies the presence of free ligand in the acidic mother liquors obtained for all methods A–C. Accordingly, in previous work, crystals of 4,4′-di-*tert*-butyl-2,2′-dipyridinium dichloride were isolated as a byproduct of the microwave-assisted reaction of **1** with water.[20]

Scheme 1. Synthesis Routes to the Octanuclear Complex $[Mo_8O_{22}(OH)_4(\text{di-}t\text{Bu-bipy})_4]$ (2)[a]

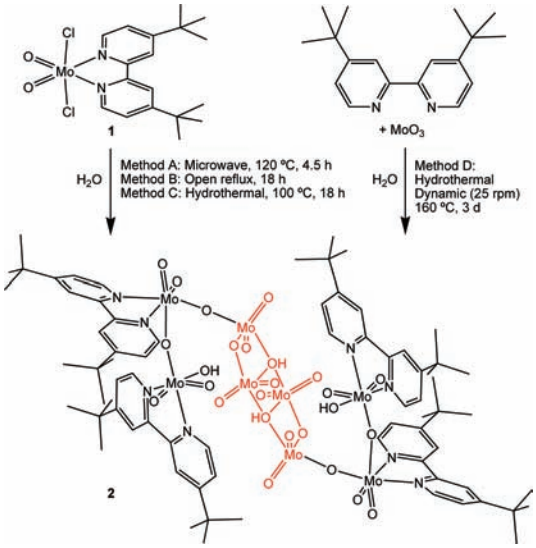

[a]The purely inorganic core $Mo_4O_8(\mu_3\text{-}OH)_2(\mu_2\text{-}O)_2$ is highlighted in red.

In common with the molecular precursor **1** and the oxodiperoxo complex $[MoO(O_2)_2(\text{di-}t\text{Bu-bipy})]$,[21] the FT-IR spectrum of **2** exhibits a strong pyridyl ring stretching vibration at 1615 cm^{-1}, which is indicative of the bidentate coordination mode of the di-*t*Bu-bipy ligands to Mo^{VI} centers. In addition, a complex pattern of bands is displayed in the 600–950 cm^{-1} range attributable to Mo–O modes. Compound **2** is slightly soluble in acetonitrile, dichloromethane, and chloroform and insoluble in water, ethanol, *n*-hexane, and diethyl ether.

Crystal Structure Description of $[Mo_8O_{22}(OH)_4(\text{di-}t\text{Bu-bipy})_4]$ (2). Because of the very small dimensions of the crystals of **2** isolated from method D, X-ray diffraction at high angles was poor, meaning that reasonably good I/σ values could not be obtained for all reflections, with this being directly translated into a high R_{int} value (Table 1) and, consequently, limitations concerning the atomic parameters of the crystal model (please see the Experimental Section for full details). Nevertheless, analysis of the available data set produced a structural model of **2** fully consistent with the other characterization data, including powder X-ray diffraction of the microcrystalline powders obtained by methods A–D (Figure S2).

Compound **2** crystallizes as discrete centrosymmetric octanuclear units, which were ultimately formulated as $[Mo_8O_{22}(OH)_4(\text{di-}t\text{Bu-bipy})_4]$. The octanuclear complex can be divided into two distinct sections (Figure 1): the inner core,

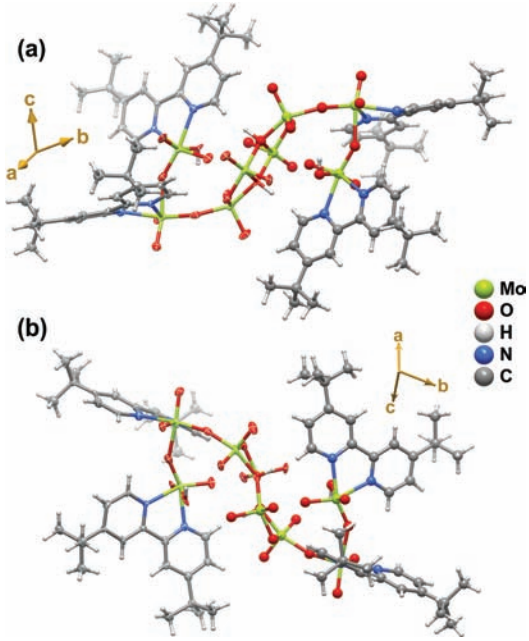

Figure 1. Schematic representation of the centrosymmetric $[Mo_8O_{22}(OH)_4(\text{di-}t\text{Bu-bipy})_4]$ molecular unit viewed in perspective along two distinct crystallographic directions. Atoms belonging to the asymmetric unit are represented as thermal ellipsoids drawn at the 30% probability level. Hydrogen atoms are represented as small spheres with arbitrary radii.

composed of four Mo centers, $Mo_4O_8(\mu_3\text{-}OH)_2(\mu_2\text{-}O)_2$, is purely inorganic and is attached to two peripheral symmetry-related oxo-bridged dinuclear units containing *N*,*N*′-chelated di-*t*Bu-bipy moieties in the coordination spheres of each metal center. Because of the considerable steric repulsion associated with these bulky organic ligands, the octanuclear complex adopts a highly distorted form strongly resembling an "S"-shaped molecular unit. The related octanuclear $[Mo_8O_{24}(\text{di-}t\text{Bu-bipy})_4]$ windmill-type complex can also be divided into an inorganic core and a surrounding hybrid sphere containing the same *N*,*N*′-chelated organic ligand.[3] However, in this latter complex, the $Mo_4(\mu_3\text{-}O)_4$ inorganic core is significantly more symmetrical, adopting the typical metal distribution of a cubane-type complex. Consequently, the peripheral Mo octahedra holding the coordinated organic ligands are uniformly distributed around the core, leading to a highly symmetrical complex.

The centrosymmetric $[Mo_8O_{22}(OH)_4(\text{di-}t\text{Bu-bipy})_4]$ complex is composed of four crystallographically independent Mo centers: Mo1 and Mo2 compose the aforementioned $Mo_4O_8(\mu_3\text{-}OH)_2(\mu_2\text{-}O)_2$ inorganic core, while Mo3 and Mo4 are peripheral to this core, each being coordinated to one *N*,*N*′-

dx.doi.org/10.1021/ic202640a | *Inorg. Chem.* 2012, 51, 3666–3676

chelated di-*t*Bu-bipy ligand (Figure 2). The Mo1 and Mo2 centers exhibit significantly distorted square pyramidal

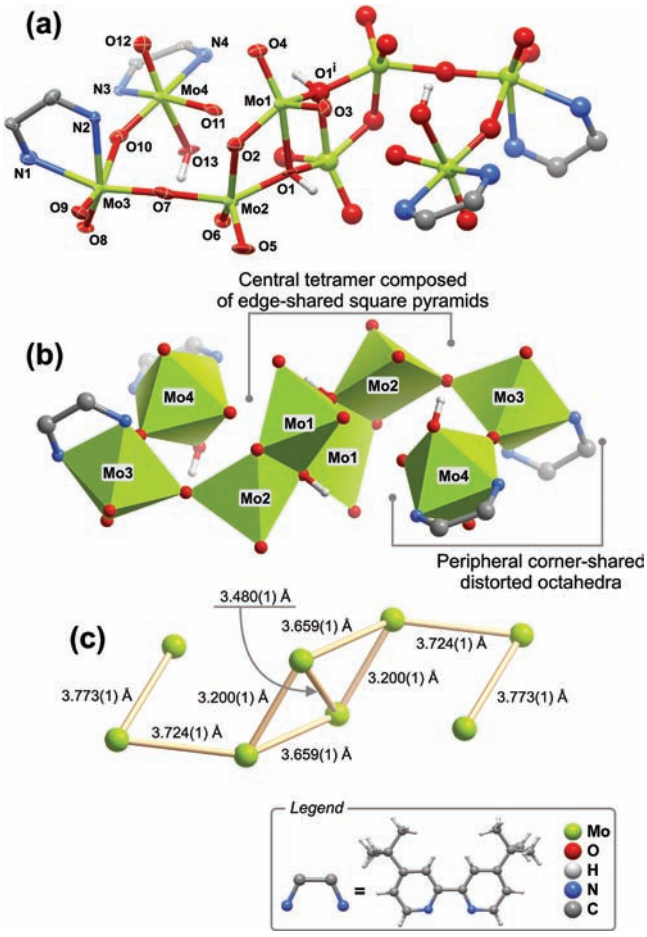

Figure 2. (a) Detailed view of the octanuclear core of the centrosymmetric $[Mo_8O_{22}(OH)_4(di\text{-}tBu\text{-}bipy)_4]$ molecular unit. Atoms belonging to the asymmetric unit are represented as thermal ellipsoids drawn at the 30% probability level. Hydrogen atoms are represented as small spheres with arbitrary radii. The labeling scheme is provided for all atoms composing the first coordination spheres of the four crystallographically independent Mo centers. (b) Polyhedral representation of the same octanuclear core. (c) Intermetallic distances of oxygen-bridged close Mo centers. For selected bond lengths and angles on the represented coordination polyhedra, see Tables 2 and 3, respectively. Symmetry transformation used to generate equivalent atoms: (i) $1 - x, 2 - y, -z$.

coordination environments with the overall Mo−O bond lengths ranging from 1.688(14) to 2.283(14) Å (Table 2 and Figure 2a), and the *cis* $O-Mo-O_{basal}$ and $O-Mo-O_{apical}$ polyhedral angles lying in the 70.9(6)−102.6(7)° and 99.8(7)−107.5(8)° ranges, respectively (Table 3). The $\{MoO_5\}$ coordination environment of Mo1 is significantly more distorted than that of Mo2 due to its close proximity to a symmetry-related (by inversion) Mo1 [Mo1···Mo1 distance of 3.480(1) Å, Figure 2c]. This creates a significant electrostatic repulsion between the two spatially close Mo cores, concomitantly leading to a highly distorted coordination environment.

The $Mo_4O_8(\mu_3\text{-}OH)_2(\mu_2\text{-}O)_2$ inorganic core is composed of a truly unique assembly of four $\{MoO_5\}$ distorted square pyramids connected to each other *via* edge-sharing, with the

Table 2. Bond Distances (in Å) for the Four Crystallographically Independent Mo Coordination Environments Present in $[Mo_8O_{22}(OH)_4(di\text{-}tBu\text{-}bipy)_4]$ (2)[a]

Mo1−O1	2.283(14)	Mo2−O1	1.935(15)
Mo1−O1^i	1.984(17)	Mo2−O2	2.073(15)
Mo1−O2	1.860(16)	Mo2−O5	1.718(16)
Mo1−O3	1.689(14)	Mo2−O6	1.720(14)
Mo1−O4	1.688(14)	Mo2−O7	1.942(17)
Mo3−O7	1.836(17)	Mo4−O10	1.764(16)
Mo3−O8	1.716(13)	Mo4−O11	1.754(15)
Mo3−O9	1.688(16)	Mo4−O12	1.683(15)
Mo3−O10	2.174(15)	Mo4−O13	2.273(15)
Mo3−N1	2.231(19)	Mo4−N3	2.264(16)
Mo3−N2	2.300(17)	Mo4−N4	2.291(19)

[a]Symmetry transformation used to generate equivalent atoms: (i) $1 - x, 2 - y, -z$.

Table 3. Bond Angles (in Degrees) for the Four Crystallographically Independent Mo Coordination Environments Present in $[Mo_8O_{22}(OH)_4(di\text{-}tBu\text{-}bipy)_4]$ (2)[a]

O1^i−Mo1−O1	70.9(6)	O1−Mo2−O2	76.5(6)
O2−Mo1−O1	72.9(6)	O1−Mo2−O7	148.2(6)
O2−Mo1−O1^i	139.7(6)	O5−Mo2−O1	106.6(7)
O3−Mo1−O2	104.2(7)	O5−Mo2−O2	104.2(7)
O3−Mo1−O1	101.6(6)	O5−Mo2−O6	107.5(8)
O3−Mo1−O1^i	99.8(7)	O5−Mo2−O7	101.6(8)
O4−Mo1−O1	153.7(6)	O6−Mo2−O1	91.6(7)
O4−Mo1−O2	102.6(7)	O6−Mo2−O2	148.1(6)
O4−Mo1−O3	104.5(7)	O6−Mo2−O7	93.7(7)
O4−Mo1−O1^i	102.1(7)	O7−Mo2−O2	82.7(6)
O7−Mo3−O10	85.8(6)	O10−Mo4−O13	90.6(6)
O7−Mo3−N1	161.2(7)	O10−Mo4−N3	87.8(6)
O7−Mo3−N2	93.4(6)	O10−Mo4−N4	157.2(7)
O8−Mo3−O7	108.2(7)	O11−Mo4−O10	105.9(7)
O8−Mo3−O10	90.4(6)	O11−Mo4−O13	83.8(6)
O8−Mo3−N1	87.2(7)	O11−Mo4−N3	151.8(7)
O8−Mo3−N2	153.3(6)	O11−Mo4−N4	89.9(7)
O9−Mo3−O7	100.1(7)	O12−Mo4−O10	103.4(7)
O9−Mo3−O8	104.1(7)	O12−Mo4−O11	107.0(7)
O9−Mo3−O10	161.6(6)	O12−Mo4−O13	158.7(6)
O9−Mo3−N1	85.9(7)	O12−Mo4−N3	93.0(6)
O9−Mo3−N2	86.8(7)	O12−Mo4−N4	87.0(7)
O10−Mo3−N1	83.4(6)	O13−Mo4−N4	74.5(6)
O10−Mo3−N2	75.4(6)	N3−Mo4−O13	71.3(5)
N1−Mo3−N2	69.0(6)	N3−Mo4−N4	71.2(6)

[a]Symmetry transformation used to generate equivalent atoms: (i) $1 - x, 2 - y, -z$.

Mo···Mo distances ranging from 3.200(1) to 3.659(1) Å (Figures 2b and c). A search in the Cambridge Structural Database (version 5.32, November 2011 with four updates)[22] revealed the existence of only a handful of structures containing edge-shared $\{MoO_5\}$ polyhedra, in particular, various assemblies of three $\{MoO_5\}$'s fused to an octahedron,[2n,23] or two $\{MoO_5\}$'s fused to two octahedra;[2g,24] however, cores based on four edge-fused $\{MoO_5\}$ units such as that found in **2** have yet to be described. Another interesting feature concerns the fact that the Mo=O apical bonds of the Mo1 and Mo2 polyhedra are *cis* to each other with respect to the mean plane of the two bases of the pyramids (Figure 2b). Even though the Mo1

dx.doi.org/10.1021/ic202640a | *Inorg. Chem.* 2012, 51, 3666−3676

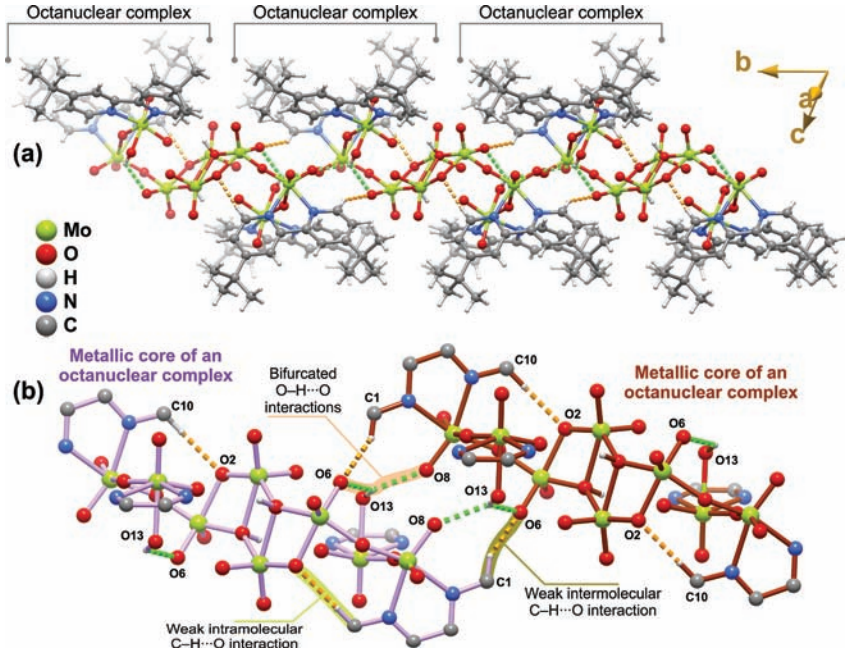

Figure 3. (a) Schematic representation of the way adjacent octanuclear $[Mo_8O_{22}(OH)_4(di\text{-}tBu\text{-}bipy)_4]$ complexes close pack along the [010] direction of the unit cell, with the process being mediated by various intra- and intermolecular weak C–H···O interactions and bifurcated O–H···O hydrogen bonds. (b) Detailed view of the supramolecular contacts present between the octanuclear core of adjacent centrosymmetric $[Mo_8O_{22}(OH)_4(di\text{-}tBu\text{-}bipy)_4]$ molecular units. For geometrical details on the represented contacts see Table 4. Symmetry codes associated with symmetry-equivalent atoms have been omitted for clarity.

coordination environment is more distorted than that of Mo2, the two Mo centers are raised from the average coordination basal planes by approximately the same distance (0.42 Å for Mo1 and 0.49 Å for Mo2).

The two remaining Mo centers, Mo3 and Mo4, exhibit highly distorted octahedral $\{MoN_2O_4\}$ coordination environments, with each being coordinated to one *N*,*N*′-chelated di-*t*Bu-bipy ligand and four oxygen-containing groups. While for Mo3 two of these oxygens belong to μ_2-bridging oxido groups [establishing connections to the inorganic core (O7) and to the neighboring Mo4 metal center (O10), Figure 2a], for Mo4 one of these groups is a terminal charge-balancing hydroxyl moiety (O13, Figure 2a). The octahedral coordination environments of Mo3 and Mo4 are highly distorted due to the presence of two Mo=O groups in their coordination spheres, which exert a marked *trans* effect on the coordination polyhedra by displacing the metal cations from their geometrical centers: for the two coordination polyhedra, while the Mo–(N,O) bond lengths range from 1.683(15) to 2.300(17) Å, the *cis* and *trans* (N,O)–Mo–(N,O) internal octahedral angles are found in the 69.0(6)–108.2(7)° and 151.8(7)–161.6(6)° ranges, respectively (Tables 2 and 3). Because the connections between adjacent $\{MoN_2O_4\}$ octahedra, and between the $Mo_4O_8(\mu_3\text{-}OH)_2(\mu_2\text{-}O)_2$ inorganic core and Mo3, are based on corner-sharing (Figure 2b), the Mo···Mo separations are concomitantly longer: 3.724(1) and 3.773(1) Å for Mo2···Mo3 and Mo3···Mo4, respectively (Figure 2c).

Despite the highly asymmetric shape of the octanuclear $[Mo_8O_{22}(OH)_4(di\text{-}tBu\text{-}bipy)_4]$ complex, the close packing of individual units is relatively efficient, being moderated by a number of supramolecular contacts. As shown in Figure 3a, individual complexes pack close in a parallel fashion along the [010] direction of the unit cell in such a way that the inorganic cores are clearly separated from the external hybrid portion of the complexes. In addition, the terminal O13 hydroxyl groups bound to Mo4 (see previous paragraph) are engaged in relatively strong O–H···O hydrogen bonding interactions with the O8 oxo groups of an adjacent inorganic core (Figure 3b). The strengths of these intercore connections are further cooperatively increased by the existence of a number of intermolecular C–H···O interactions: for example, the C1 atom of a coordinated di-*t*Bu-bipy ligand interacts with the O6 oxido group *via* a strong [$d_{C\cdots O}$ = 3.17(2) Å] and relatively directional [∠(CHO) = 146°] contact. A number of weak intramolecular C–H···O contacts also exist in the crystal structure, with the most relevant being tabulated in Table 4. The overall combination of all of these supramolecular contacts leads to the formation of robust one-dimensional chains running parallel to the *b*-axis of the unit cell. Individual chains close pack in the *ac* plane mediated by purely geometrical reasons because the contacts between spatially close di-*t*Bu-bipy organic molecules are, essentially, of the van der Waals type (Figure 4).

Table 4. Hydrogen Bonding and Close Contact (Both Inter- and Intramolecular) Geometrical Details (Distances in Å and Angles in Degrees) for $[Mo_8O_{22}(OH)_4(di\text{-}tBu\text{-}bipy)_4]$ (2)[a]

D–H···A	*d*(D···A)	∠(DHA)
O13–H13···O2^{i}	2.73(2)	121
O13–H13···O6	2.93(2)	124
C10–H10···O2 (*intramolecular*)	3.28(2)	169
C1–H1···O6^{i} (*intermolecular*)	3.17(2)	146
C7–H7···O9^{ii} (*intermolecular*)	3.05(2)	127
C16–H16C···O9^{ii} (*intermolecular*)	3.43(2)	165
C32–H32B···O4^{iii} (*intermolecular*)	3.49(2)	153

[a]Symmetry transformations used to generate equivalent atoms: (i) 1 − *x*, 1 − *y*, −*z*; (ii) 2 − *x*, 1 − *y*, −*z*; (iii) 1 − *x*, 1 − *y*, 1 − *z*.

dx.doi.org/10.1021/ic202640a | *Inorg. Chem.* 2012, 51, 3666–3676

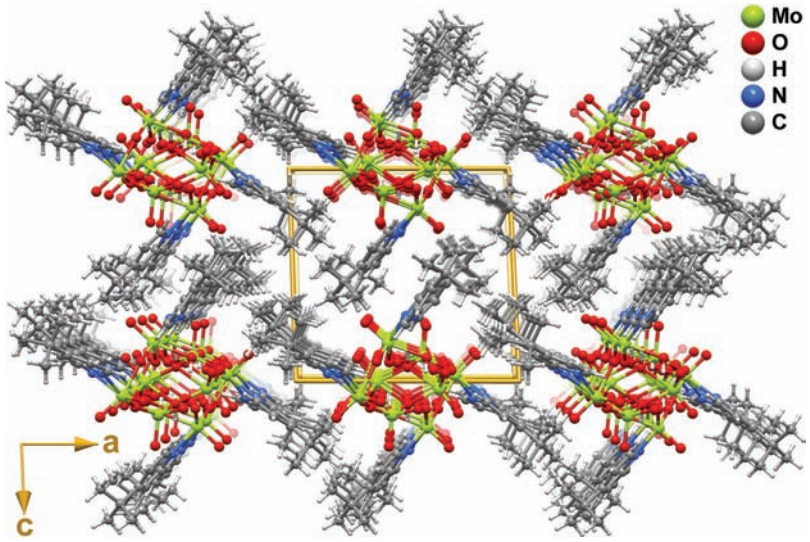

Figure 4. Crystal packing of the $[Mo_8O_{22}(OH)_4(di\text{-}tBu\text{-}bipy)_4]$ compound viewed in perspective along the [010] direction of the unit cell. Weak C–H···O interactions and O–H···O hydrogen bonds, which mediate the crystal packing along the *b*-axis, have been omitted for clarity.

Catalytic Epoxidation of Bioderived Olefins. The Reaction of DL-Limonene. Complex **2** was applied in the catalytic epoxidation of DL-limonene (Lim), one of the most common naturally occurring monoterpenes (present in citrus oil), to give 1,2-epoxy-*p*-menth-8-ene (LimOx, Scheme 2),

Scheme 2. Epoxidation Reactions Studied in This Work

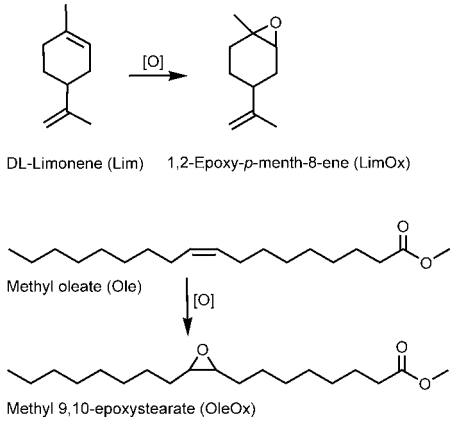

which is an interesting cycloaliphatic epoxide for the synthesis of pharmaceuticals, fragrances, and food additives; the manufacture of copolymers by reaction with CO_2; and applications in metal coatings and varnishes.[7a,25]

The systems TBHPdec/no cosolvent, TBHPdec/DCE, and TBHP/DCE (please see the Experimental Section for details) gave comparable conversions of Lim after 6 h/24 h of reaction, and LimOx was always the main product formed in similar amounts at 24 h (84–89% selectivity at 94–96% conversion, reached at 24 h, Figure 5); without a catalyst, LimOx was formed in less than 4% yield after 24 h of reaction. A comparison of the TBHPdec/no cosolvent and TBHPdec/DCE systems indicates no significant dilution effects on the observed catalytic activity. For the TBHPdec/BTF system, the initial reaction rate of Lim was lower than that observed for TBHPdec/DCE, although similarly high conversions were reached after 6 h; LimOx and 1,2:8,9-diepoxy-*p*-menthane (LimDiOx) were formed in 76% and 22% yield at 98% conversion and 24 h reaction (no LimDiol was detected). For the two solvents, the reaction mixtures were biphasic liquid–solid. Differences in the solvent polarity may influence the solubility of the metal species, and consequently the reaction rate (based on the dipole moment, BTF (2.86 D) is slightly more polar than that for DCE (1.83 D)). For the system TBHP/DCE (in which the oxidant solution was prepared by mixing 70% aqueous TBHP and DCE, followed by the removal of excess water using $MgSO_4$), LimDiOx was formed in 8% yield at 24 h (Figure 5B). These results indicate very high regioselectivity toward the epoxidation of the endocyclic double bond relative to the exocyclic one. The selectivity to LimOx tends to decrease for conversions of Lim greater than ca. 80% (Figure 5B): for all tested reaction systems excluding TBHPdec/BTF, this trend is accompanied by the formation of 1-methyl-4-(1-methylethenyl)-1,2-cyclohexanediol (denoted LimDiol), reaching a maximum yield at 24 h of 11% for the TBHPdec/no cosolvent system. For TBHPdec/BTF, the decrease in selectivity to LimOx was accompanied by the formation of LimDiOx (no LimDiol was detected). The decrease in LimOx selectivity and concomitant increase in selectivities to LimDiol and LimDiOx (TBHP/DCE system, Figure 5B) suggest that LimOx is a common intermediate product in the formation of LimDiol and LimDiOx. The formation of LimDiol may take place via the hydrolysis of LimOx with residual water present in the reaction media. Accordingly, the presence of water influences the product distribution by favoring the LimOx to LimDiol conversion, which may take place in parallel with the LimOx to LimDiOx conversion. The comparable LimOx yields at 24 h for the three oxidant/solvent systems suggest that it may be feasible to use TBHPaq (coupled with a drying procedure) instead of TBHPdec and to substitute decane (bp ca. 174 °C) for solvents with lower boiling points, thereby avoiding energy-intensive separation/purification processes.

The catalytic performance of **2** was compared with those for MoO_3 (freshly prepared by using MoO_2Cl_2 as the source of molybdenum and following the conditions used in method D, omitting the organic ligand) and a commercial ammonium heptamolybdate ($(NH_4)_6Mo_7O_{24}\cdot 4H_2O$, 99% p.a., Merck), under similar reaction conditions using the system

dx.doi.org/10.1021/ic202640a | *Inorg. Chem.* 2012, 51, 3666–3676

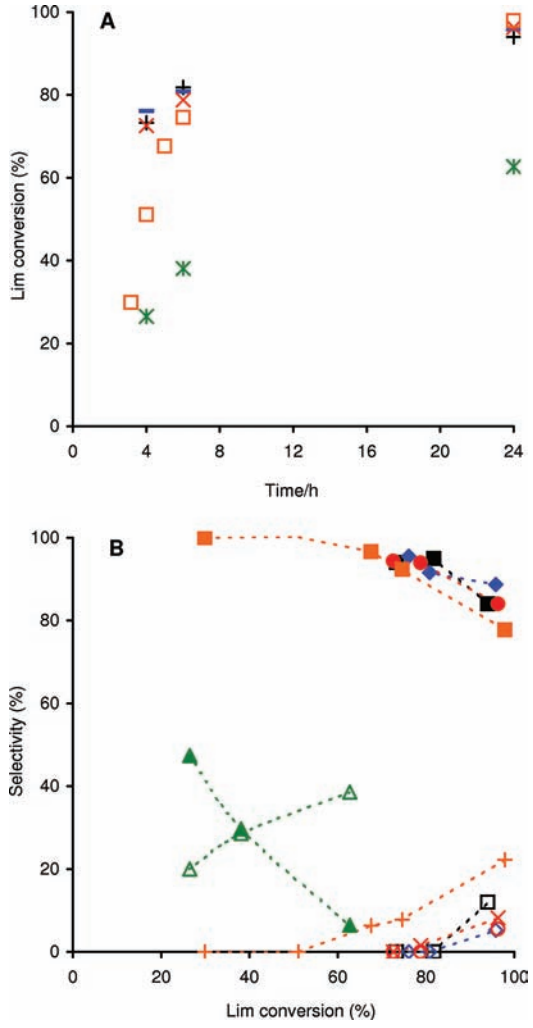

Figure 5. (A) Kinetic profiles for the reaction of DL-limonene (Lim) at 55 °C using the systems TBHPdec/no cosolvent (black +), TBHPdec/BTF (orange □), TBHPdec/DCE (blue —), TBHP/DCE (red ×), and TBHP/EtOH (green *). (B) Dependence of selectivity to LimOx (solid-filled symbols), LimDiol (white-filled symbols), and LimDiOx (+,×) on Lim conversion using the systems TBHPdec/no cosolvent (■,□), TBHPdec/BTF (orange ■,+), TBHPdec/DCE (blue ♦,◊), TBHP/DCE (red ●,○,×), and TBHP/EtOH (green ▲,△).

TBHPdec/DCE. After 6 h of reaction, conversion of Lim was negligible for both MoO_3 and the heptamolybdate. When compared against previously investigated oxomolybdenum complexes or their carbonyl precursors tested as catalysts in the same reaction, using TBHP as an oxidant at 55 °C, the catalytic performance of complex **2** seems quite outstanding in terms of the LimOx yield reached (at 24 h, unless otherwise stated): $[MoO_2X_2L_2]$ (for X = Cl, LimOx yields of 39% for L = dimethylformamide,[26] 74% for L = {$OP(CH_2CH_3)(Ph)_2$},[27] 65% for L_2 = bidentate salen ligand,[28] 15–20% for L_2 = {$PhCHNCH_2CH_2NCHPh$};[29] for X = CH_3, LimOx yield of 47% at 4 h for L_2 = *N*,*N*-p-tolyl-2,3-dimethyl-1,4-diazabutadiene[30]); $[MoO_2L]$ where L is a tetradentate oxazoline ligand[31] (59% LimOx yield) or a tetradentate salen ligand[28] (50% LimOx yield); $[CpMo(CO)_nL]$ where *n* = 2 and L = η^3-C_3H_5 (70% of LimOx plus LimDiOx)[32] or *n* = 3 and L = Cl (21% LimOx yield at 6 h);[33] $[Mo_2O_4(\mu_2\text{-}O)Cl_2(pyrazole)_4]$ (59% LimOx yield at 6 h).[34] High LimOx yields have been reported in a few cases: 88% LimOx yield at 24 h/55 °C for $[Mo(CO)_4$(ethyl[3-(2-pyridyl)-1-pyrazolyl]acetate}],[4] 82% LimOx yield at 35 min for $[(\eta^5\text{-}C_9H_7)Mo(CO)_3Me]$,[35] and 95–100% LimOx yield at 24 h/55 °C for $[MoO_2X_2L_2]$, where X = Cl or $OSiPh_3$ and L_2 = 2-(1-butyl-3-pyrazolyl)pyridine).[36]

With the aim of replacing DCE or BTF with a more environmentally attractive, bioderived solvent, the epoxidation of Lim was carried out using the system TBHP/EtOH, complex **2**, and a reaction temperature of 55 °C. The reaction of Lim was considerably slower for TBHP/EtOH than for TBHP/DCE (Figure 5A), and selectivity to LimOx decreased from 47% at 27% conversion to 6% at 63% conversion (reached at 24 h reaction), with the concomitant formation of several byproducts including LimDiol (39% selectivity at 63% conversion, Figure 5B); without a catalyst, less than 3% Lim conversion was reached at 24 h under similar reaction conditions. A possible explanation for the slower reaction of Lim when EtOH is used as a cosolvent instead of (non-coordinating) DCE is that the EtOH molecules may compete with the reagents in the coordination to the metal center.[37] It is worth mentioning that for the two solvents the reaction mixtures were similarly biphasic liquid–solid. The enhanced formation of LimDiol for the system TBHP/EtOH may be partly due to the less efficient removal of water from this mixture prior to the catalytic reaction. Besides LimDiol, ethoxy alcohol products were formed possibly via the ethanolysis of the epoxide products. The formation of ethoxy alcohol products has been reported for the reaction of LimOx with ethanol in the presence of $BF_3{\cdot}O(C_2H_5)_2$ or EtONa.[38]

The tested reaction systems were always biphasic solid–liquid, and the ATR FT-IR spectra of the recovered solids were similar to that of the fresh catalyst (Figure S3). The solid recovered from the catalytic reaction using the system TBHPdec/DCE was reused in a second 24 h batch run, under similar reaction conditions, giving comparable conversion (74%/95%) and LimOx selectivity (89%/88%) at 6 h/24 h to those observed for run 1 (92%/89% LimOx selectivity at 79%/96% conversion). The "productive consumption" of TBHP was ascertained by iodometric titrations, which indicated no measurable decomposition of TBHP (to give *tert*-butanol and molecular oxygen) in the presence of **2** (without olefin), at 55 °C.

The homogeneous/heterogeneous nature of the catalytic reaction performed using the system TBHP/DCE was checked by filtering the reaction mixture through a 0.2 μm PTFE membrane after 1 h and then leaving the filtrate to react at 55 °C for a further 5 h. The increment in conversion between 1 and 6 h was 32%, which is comparable to that observed in the presence of the solid (36%). Hence, the catalytic reaction takes place in the homogeneous phase. Compound **2** did not dissolve completely even when the amount charged to the reactor was decreased from 1 mol % (Mo/Lim) to 0.2 mol %. Unsurprisingly, therefore the kinetic behavior of the homogeneous phase catalytic reaction using 0.2 mol % was similar (94%/91% LimOx selectivity at 74%/91% conversion for 6 h/24 h) to that measured for 1 mol % (94%/84% LimOx selectivity at 79%/96% conversion).

The Reaction of Methyl Oleate. Fatty acid methyl ester epoxides are bioderived oleochemicals with a significant impact in the chemical industry due to their wide applications profile, e.g., as plasticizers and stabilizers in the production of polyvinyl chloride (PVC), as plastic additives, and as intermediates in the production of biodegradable lubricants and polyols for

dx.doi.org/10.1021/ic202640a | *Inorg. Chem.* 2012, 51, 3666–3676

polyurethane production.[7a,b,39] The industrial scale epoxidation of unsaturated plant oils is carried out by the Prileshajev reaction using either preformed or *in situ* generated short chain peroxyacids (e.g., peracetic acid) which react with the unsaturated fatty acid C=C double bond to give the corresponding epoxide.[7a] Some drawbacks of this process include the wide range of byproducts formed (which result in more demanding separation/purification steps and enhanced formation of waste products), equipment corrosion hazards (presence of strong acid in an oxidative environment), and the need for neutralization processes downstream. A potentially interesting alternative that may render the epoxidation of vegetable oils more selective is the use of catalysts based on high-valent transition metals such as molybdenum(VI).[7c,d,39b]

The catalytic potential of **2** for the production of biobased epoxidized vegetable oils was investigated using methyl oleate (denoted Ole) as a model substrate, which is a monounsaturated fatty acid ester present in, for example, methyl oleate soybean oil. The oxygen donor was TBHPdec, and the cosolvent was DCE, BTF, EtOAc, or CH_3CN, at 55 °C. The main reaction product was always methyl 9,10-epoxystearate (OleOx) formed in at least 91% selectivity at high conversions (up to 94%, Figure 6); without a catalyst, no reaction occurred under similar reaction conditions. The highest initial catalytic activity was observed for DCE as a cosolvent, and BTF led to the highest OleOx yield (92%) at high conversion (99% OleOx selectivity at 94% conversion, reached at 24 h reaction). When EtOAc or CH_3CN was used as a cosolvent, the OleOx selectivity was 95−97% at ca. 60% conversion (24 h reaction). As found with Lim as the substrate, these reaction systems were always biphasic solid−liquid, and the ATR FT-IR spectra of the solids recovered after a 24 h batch run were similar to that of **2** (Figure S3). The slower reaction for the cosolvents EtOAc and CH_3CN may be due to their ability to compete with the reagents in the coordination to the metal center, in parallel with that discussed above for EtOH as cosolvent in the reaction of Lim.

To the best of our knowledge, the epoxidation of pure methyl oleate using molybdenum-based catalytic systems has not been reported. Wang and co-workers reported that the epoxidation of a mixture of methyl oleate and methyl lineolate with $H_2O_2/NaHCO_3$ in the presence of the complex $[MoO(O_2)_2(8\text{-quinilinol})_2]$ gave 92% total selectivity to epoxides at 72% conversion, using CH_3CN as a cosolvent, at 2 h/30 °C.[7d] Sobczak and Ziółkowski investigated the epoxidation of oleic acid with organic hydroperoxides in the presence of the complexes $[Mo(CO)_6]$, $H_2[Mo_2O_4(oxalate)_2(H_2O)_2]\cdot 4H_2O\cdot(CH_3)_2CO$, $[MoO_2(acac)_2]$, and $[MoO_2(SAP)(EtOH)]$ (SAP = dianionic tridentate salycylideneiminophenolate chelating ligand); the latter complex exhibited the best catalytic performance, giving ca. 87% epoxide selectivity at 67% TBHP conversion, at 260 min/80 °C.[7e] More recently, it was reported that the use of $[MoO_2(acac)_2]$ as a catalyst in the epoxidation of soybean oil with TBHP led to 77% epoxide selectivity at 70% conversion (2 h/110 °C).[7c]

The structure of compound **2** consists of a type of clustered molybdenum oxide/organic assembly, and therefore steric effects may partly explain the higher reactivity of Lim in comparison to the bulkier substrate Ole, under similar reaction conditions (TBHPdec/DCE). On the other hand, these structural features of **2** may hinder catalyst autodegradation pathways, which may partly explain the fairly high catalyst stability observed.

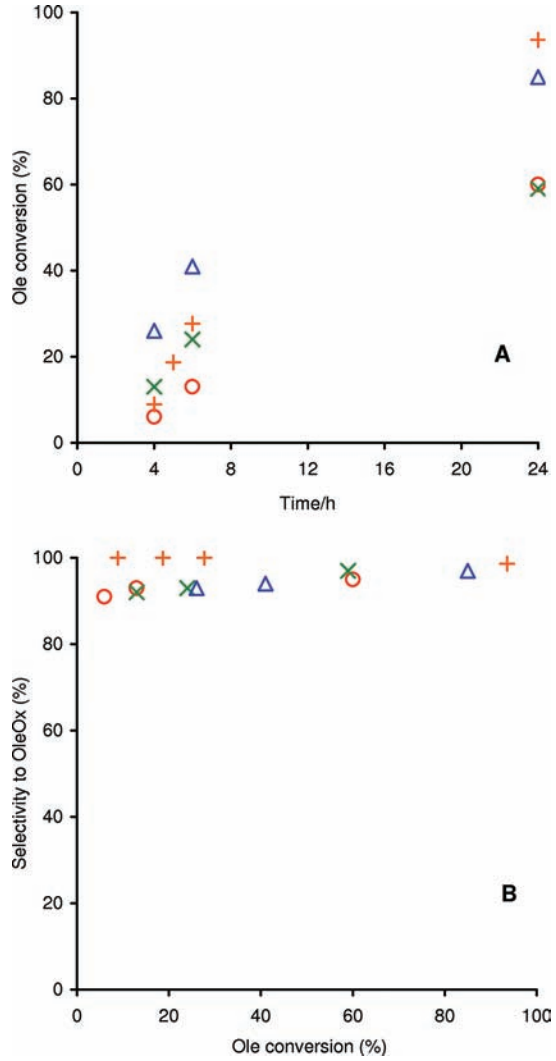

Figure 6. (A) Kinetic profiles for the reaction of methyl oleate (Ole), and (B) dependence of selectivity to OleOx on Ole conversion, using the systems TBHPdec/DCE (blue △), TBHPdec/BTF (orange +), TBHPdec/EtOAc (red ○), and TBHPdec/CH_3CN (green ×).

CONCLUSIONS

The present work has reinforced the notion that the hydrolysis and condensation of complexes of the type $[MoO_2Cl_2L]$ is a potentially interesting route to molybdenum oxide/organic assemblies with structures and properties directed to a large extent by the type of organic ligand and its substituents. Thus, for reactions with water at 100−120 °C, the hybrid molybdenum oxide/bipyridine material $\{[MoO_3(2,2'\text{-bipy})]\text{-}[MoO_3(H_2O)]\}_n$ is obtained with L = 2,2′-bipyridine, while the octanuclear species $[Mo_8O_{22}(OH)_4(\text{di-}t\text{Bu-bipy})_4]$ (**2**) is obtained with L = 4,4′-di-*tert*-butyl-2,2′-bipyridine. The $Mo_4O_8(\mu_3\text{-}OH)_2(\mu_2\text{-}O)_2$ inorganic core in **2** is composed of a truly unique assembly of four $\{MoO_5\}$ distorted square pyramids connected to each other *via* edge-sharing. In a manner analogous to that commonly used in sol−gel chemistry, hydrolysis of the Mo−Cl bonds in the molecular precursors likely gives reactive Mo−OH species that condense through oxolation and/or olation reactions to give metal-oxo clusters,

dx.doi.org/10.1021/ic202640a | *Inorg. Chem.* 2012, 51, 3666−3676

oligomers, and polymers assembled via M−O−M and/or M−OH−M bridges. Ongoing work in our laboratories has indicated that a wide range of structurally diverse compounds are accessible by using this approach. These molybdenum oxide/organic assemblies are promising catalysts for the epoxidation of nonfunctionalized olefins, such as the conversion of bioderived olefins into added value epoxides studied in the present work.

■ ASSOCIATED CONTENT

Ⓢ Supporting Information

Crystallographic information file (CIF) for compound **2**, FT-IR and powder XRD patterns of **2** synthesized by methods A−D, and ATR FT-IR spectra of the solids recovered at the end of the catalytic runs. This material is available free of charge via the Internet at http://pubs.acs.org.

■ AUTHOR INFORMATION

Corresponding Author

*E-mail: igoncalves@ua.pt.

Notes

The authors declare no competing financial interest.

■ ACKNOWLEDGMENTS

We are grateful to the Fundação para a Ciência e a Tecnologia (FCT), the Programa Operacional Ciência e Inovação (POCI) 2010, Orçamento do Estado (OE), and Fundo Europeu de Desenvolvimento Regional (FEDER) for general funding (project PTDC/QUI/65427/2006) and for financial support (FCT) towards the purchase of the single-crystal diffractometer. We acknowledge the FCT for a Ph.D. grant to T.R.A. (SFRH/BD/64224/2009) and a postdoctoral grant to P.N. (SFRH/BPD/73540/2010).

■ REFERENCES

(1) (a) Hagrman, P. J.; Hagrman, D.; Zubieta, J. *Angew. Chem., Int. Ed.* **1999**, *38*, 2638. (b) Hagrman, D.; Hagrman, P. J.; Zubieta, J. *Comments Inorg. Chem.* **1999**, *21*, 225.

(2) (a) Zapf, P. J.; Haushalter, R. C.; Zubieta, J. *Chem. Mater.* **1997**, *9*, 2019. (b) Kim, J.; Lim, W. T.; Koo, B. K. *Inorg. Chim. Acta* **2007**, *360*, 2187. (c) Lu, Y.; Wang, E.; Yuan, M.; Li, Y.; Hu, C. *J. Mol. Struct.* **2003**, *649*, 191. (d) Hagrman, P. J.; LaDuca, R. L. Jr.; Koo, H.-J.; Rarig, R. Jr.; Haushalter, R. C.; Whangbo, M.-H.; Zubieta, J. *Inorg. Chem.* **2000**, *39*, 4311. (e) Cui, C.-P.; Dai, J.-C.; Du, W.-X.; Fu, Z.-Y.; Hu, S.-M.; Wu, L.-M.; Wu, X.-T. *Polyhedron* **2002**, *21*, 175. (f) Niu, J.; Wang, Z.; Wang, J. *Inorg. Chem. Commun.* **2004**, *7*, 556. (g) Zapf, P. J.; LaDuca, R. L. Jr.; Rarig, R. S. Jr.; Johnson, K. M. III; Zubieta, J. *Inorg. Chem.* **1998**, *37*, 3411. (h) Zhou, Y.; Zhang, L.; Fun, H.-K.; You, X. *Inorg. Chem. Commun.* **2000**, *3*, 114. (i) Li, D.; Liu, Y.; Wei, P.; Hu, B.; Zhang, X. *Acta Crystallogr., Sect. E: Struct. Rep. Online* **2009**, *E65*, m1074. (j) Xu, Y.; Lu, J.; Goh, N. K. *J. Mater. Chem.* **1999**, *9*, 1599. (k) Rarig, R. S. Jr.; Zubieta, J. *Inorg. Chim. Acta* **2001**, *312*, 188. (l) Chuang, J.; Ouellette, W.; Zubieta, J. *Inorg. Chim. Acta* **2008**, *361*, 2357. (m) Lysenko, A. B.; Senchyk, G. A.; Lincke, J.; Lässig, D.; Fokin, A. A.; Butova, E. D.; Schreiner, P. R.; Krautscheid, H.; Domasevitch, K. V. *Dalton Trans.* **2010**, *39*, 4223. (n) Hagrman, D.; Zubieta, C.; Rose, D. J.; Zubieta, J.; Haushalter, R. C. *Angew. Chem., Int. Ed. Engl.* **1997**, *36*, 873. (o) Zapf, P. J.; Warren, C. J.; Haushalter, R. C.; Zubieta, J. *Chem. Commun.* **1997**, 1543. (p) Hagrman, D.; Zapf, P. J.; Zubieta, J. *Chem. Commun.* **1998**, 1283. (q) Hagrman, D.; Sangregorio, C.; O'Connor, C. J.; Zubieta, J. *J. Chem. Soc., Dalton Trans.* **1998**, 3707. (r) Hagrman, P. J.; Zubieta, J. *Inorg. Chem.* **2000**, *39*, 5218. (s) Rarig, R. S. Jr.; Lam, R.; Zavalij, P. Y.; Ngala, J. K.; LaDuca, R. L. Jr.; Greedan, J. E.; Zubieta, J. *Inorg. Chem.* **2002**, *41*, 2124. (t) Kong, Z.; Weng, L.; Tan, D.; He, H.; Zhang, B.; Kong, J.; Yue, B. *Inorg. Chem.* **2004**, *43*, 5676. (u) Coué, V.; Dessapt, R.; Bujoli-Doeuff, M.; Evain, M.; Jobic, S. *Inorg. Chem.* **2007**, *46*, 2824. (v) Yang, M.-X.; Chen, L.-J.; Lin, S.; Chen, X.-H.; Huang, H. *Dalton Trans.* **2011**, *40*, 1866.

(3) Amarante, T. R.; Neves, P.; Coelho, A. C.; Gago, S.; Valente, A. A.; Paz, F. A. A.; Pillinger, M.; Gonçalves, I. S. *Organometallics* **2010**, *29*, 883.

(4) Neves, P.; Amarante, T. R.; Gomes, A. C.; Coelho, A. C.; Gago, S.; Pillinger, M.; Gonçalves, I. S.; Silva, C. M.; Valente, A. A. *Appl. Catal. A: Gen* **2011**, *395*, 71.

(5) Abrantes, M.; Amarante, T. R.; Antunes, M. M.; Gago, S.; Paz, F. A. A.; Margiolaki, I.; Rodrigues, A. E.; Pillinger, M.; Valente, A. A.; Gonçalves, I. S. *Inorg. Chem.* **2010**, *49*, 6865.

(6) (a) Arzoumanian, H.; Agrifoglio, G.; Krentzien, H.; Capparelli, M. *J. Chem. Soc. Chem. Commun.* **1995**, 655. (b) Arzoumanian, H.; Agrifoglio, G.; Krentzien, H. *New J. Chem.* **1996**, *20*, 699. (c) Arzoumanian, H.; Maurino, L.; Agrifoglio, G. *J. Mol. Catal. A: Chem.* **1997**, *117*, 471. (d) Monteiro, B.; Gago, S.; Neves, P.; Valente, A. A.; Gonçalves, I. S.; Pereira, C. C. L.; Silva, C. M.; Pillinger, M. *Catal. Lett.* **2009**, *129*, 350. (e) Ferreira, P.; Xue, W.-M.; Bencze, É.; Herdtweck, E.; Kühn, F. E. *Inorg. Chem.* **2001**, *40*, 5834. (f) Kühn, F. E.; Xue, W.-M.; Al-Ajlouni, A.; Santos, A. M.; Zang, S.; Romão, C. C.; Eickerling, G.; Herdtweck, E. *Inorg. Chem.* **2002**, *41*, 4468. (g) Kodama, S.; Nomoto, A.; Yano, S.; Ueshima, M.; Ogawa, A. *Inorg. Chem.* **2011**, *50*, 9942. (h) Kodama, S.; Hashidate, S.; Nomoto, A.; Yano, S.; Ueshima, M.; Ogawa, A. *Chem. Lett.* **2011**, *40*, 495.

(7) (a) Corma, A.; Iborra, S.; Velty, A. *Chem. Rev.* **2007**, *107*, 2411. (b) Meier, M. A. R.; Metzger, J. O.; Schubert, U. S. *Chem. Soc. Rev.* **2007**, *36*, 1788. (c) Farias, M.; Martinelli, M.; Bottega, D. P. *Appl. Catal. A: Gen.* **2010**, *384*, 213. (d) Cai, S.-F.; Wang, L.-S.; Fan, C.-L. *Molecules* **2009**, *14*, 2935. (e) Sobczak, J. M.; Ziółkowski, J. J. *Appl. Catal. A: Gen.* **2003**, *248*, 261.

(8) Monteiro, B.; Gago, S.; Neves, P.; Valente, A. A.; Gonçalves, I. S.; Pereira, C. C. L.; Silva, C. M.; Pillinger, M. *Catal. Lett.* **2009**, *129*, 350.

(9) Kottke, T.; Stalke, D. *J. Appl. Crystallogr.* **1993**, *26*, 615.

(10) *APEX2, Data Collection Software*, version 2.1-RC13; Bruker AXS; Delft, The Netherlands, 2006.

(11) *Cryopad, Remote monitoring and control*, version 1.451; Oxford Cryosystems: Oxford, UK, 2006.

(12) *SAINT+, Data Integration Engine*, version 7.23a; Bruker AXS: Madison, WI, 2005.

(13) Sheldrick, G. M. *SADABS, Bruker/Siemens Area Detector Absorption Correction Program*, version 2.01; Bruker AXS: Madison, WI, 1998.

(14) (a) Sheldrick, G. M. *Acta Crystallogr., Sect. A: Found. Crystallogr.* **2008**, *64*, 112. (b) Sheldrick, G. M. *SHELXS-97, Program for Crystal Structure Solution*; University of Göttingen: Göttingen, Germany, 1997.

(15) Sheldrick, G. M. *SHELXL-97, Program for Crystal Structure Refinement*; University of Göttingen: Göttingen, Germany, 1997.

(16) Brese, N. E.; O'Keeffe, M. *Acta Crystallogr., Sect. B: Struct. Sci.* **1991**, *47*, 192.

(17) Brown, I. D.; Altermatt, D. *Acta Crystallogr., Sect. B: Struct. Sci.* **1985**, *41*, 244.

(18) (a) Spek, A. L. *Acta Crystallogr., Sect. A: Found. Crystallogr.* **1990**, *46*, C34. (b) Spek, A. L. *J. Appl. Crystallogr.* **2003**, *36*, 7.

(19) A minor product of method D is the water-soluble complex $[\{MoO_2(\mu\text{-}O)(\text{di-}t\text{Bu-bipy})\}_2]$, which can be reproducibly isolated in very low yields by evaporation of the filtered reaction solution. Details of the crystal structure and spectroscopic characterization of the dinuclear complex will appear in a separate publication.

(20) Amarante, T. R.; Gonçalves, I. S.; Paz, F. A. A. *Acta Crystallogr., Sect. E: Struct. Rep. Online* **2011**, *67*, o1903.

(21) Amarante, T. R.; Paz, F. A. A.; Gago, S.; Gonçalves, I. S.; Pillinger, M.; Rodrigues, A. E.; Abrantes, M. *Molecules* **2009**, *14*, 3610.

(22) (a) Allen, F. H. *Acta Crystallogr., Sect. B: Struct. Sci.* **2002**, *58*, 380. (b) Allen, F. H.; Motherwell, W. D. S. *Acta Crystallogr., Sect. B: Struct. Sci.* **2002**, *58*, 407.

(23) (a) Allis, D. G.; Rarig, R. S.; Burkholder, E.; Zubieta, J. *J. Mol. Struct.* **2004**, *688*, 11. (b) Quintal, S. M. O.; Nogueira, H. I. S.; Carapuça, H. M.; Félix, V.; Drew, M. G. B. *J. Chem. Soc., Dalton Trans.*

2001, 3196. (c) Rarig, R. S.; Zubieta, J. *Polyhedron* **2003**, *22*, 177. (d) Xu, J. Q.; Wang, R. Z.; Yang, G. Y.; Xing, Y. H.; Li, D. M.; Bu, W. M.; Ye, L.; Fan, Y. G.; Yang, G. D.; Xing, Y.; Lin, Y. H.; Jia, H. Q. *Chem. Commun.* **1999**, 983.

(24) (a) Cui, X. B.; Lu, K.; Fan, Y.; Xu, J. Q.; Ye, L.; Sun, Y. H.; Li, Y.; Yu, H. H.; Yi, Z. H. *J. Mol. Struct.* **2005**, *743*, 151. (b) Lu, J.; Li, Y. G.; Shen, E. H.; Yuan, M.; Wang, E.; Hu, C. W.; Xu, L. *J. Solid State Chem.* **2004**, *177*, 1771. (c) Liang, H.; Chen, Z. F.; Hu, R. X.; Yu, Q.; Zhou, Z. Y.; Zhou, X. G. *Trans. Met. Chem* **2002**, *27*, 102. (d) Finn, R. C.; Rarig, R. S.; Zubieta, J. *Inorg. Chem.* **2002**, *41*, 2109. (e) Finn, R. C.; Zubieta, J. *Inorg. Chem.* **2001**, *40*, 2466.

(25) Byrne, C. M.; Allen, S. D.; Lobkovsky, E. B.; Coates, G. W. *J. Am. Chem. Soc.* **2004**, *126*, 11404.

(26) Monteiro, B.; Balula, S. S.; Gago, S.; Grosso, C.; Figueiredo, S.; Lopes, A. D.; Valente, A. A.; Pillinger, M.; Lourenço, J. P.; Gonçalves, I. S. *J. Mol. Catal. A: Chem.* **2009**, *297*, 110.

(27) Castro, A.; Alonso, J. C.; Valente, A. A.; Neves, P.; Brandão, P.; Félix, V.; Ferreira, P. *Eur. J. Inorg. Chem.* **2010**, 1405.

(28) Bruno, S. M.; Balula, S. S.; Valente, A. A.; Paz, F. A. A.; Pillinger, M.; Sousa, C.; Klinowski, J.; Freire, C.; Ribeiro-Claro, P.; Gonçalves, I. S. *J. Mol. Catal. A: Chem.* **2007**, *270*, 185.

(29) Petrovski, Z.; Pillinger, M.; Valente, A. A.; Gonçalves, I. S.; Hazell, A.; Romão, C. C. *J. Mol. Catal. A: Chem.* **2005**, *227*, 67.

(30) Valente, A. A.; Moreira, J.; Lopes, A. D.; Pillinger, M.; Nunes, C. D.; Romão, C. C.; Kühn, F. E.; Gonçalves, I. S. *New J. Chem.* **2004**, *28*, 308.

(31) Neves, P.; Gago, S.; Pereira, C. C. L.; Figueiredo, S.; Lemos, A.; Lopes, A. D.; Gonçalves, I. S.; Pillinger, M.; Silva, C. M.; Valente, A. A. *Catal. Lett.* **2009**, *132*, 94.

(32) Neves, P.; Pereira, C. C. L.; Paz, F. A. A.; Gago, S.; Pillinger, M.; Silva, C. M.; Valente, A. A.; Romão, C. C.; Gonçalves, I. S. *J. Organomet. Chem.* **2010**, *695*, 2311.

(33) Valente, A. A.; Seixas, J. D.; Gonçalves, I. S.; Abrantes, M.; Pillinger, M.; Romão, C. C. *Catal. Lett.* **2005**, *101*, 127.

(34) Pereira, C. C. L.; Balula, S. S.; Paz, F. A. A.; Valente, A. A.; Pillinger, M.; Klinowski, J.; Gonçalves, I. S. *Inorg. Chem.* **2007**, *46*, 8508.

(35) Abrantes, M.; Bruno, S. M.; Tomé, C.; Pillinger, M.; Gonçalves, I. S.; Valente, A. A. *Catal. Commun.* **2011**, *15*, 64.

(36) Bruno, S. M.; Pereira, C. C. L.; Balula, M. S.; Nolasco, M.; Valente, A. A.; Hazell, A.; Pillinger, M.; Ribeiro-Claro, P.; Gonçalves, I. S. *J. Mol. Catal. A: Chem.* **2007**, *261*, 79.

(37) (a) Kühn, F. E.; Groarke, M.; Bencze, E.; Herdtweck, E.; Prazeres, A.; Santos, A. M.; Calhorda, M. J.; Romão, C. C.; Gonçalves, I. S.; Lopes, A. D.; Pillinger, M. *Chem.—Eur. J.* **2002**, *8*, 2370. (b) Veiros, L. F.; Prazeres, A.; Costa, P. J.; Romão, C. C.; Kühn, F. E.; Calhorda, M. J. *Dalton Trans.* **2006**, 1383. (c) Al-Ajlouni, A.; Valente, A. A.; Nunes, C. D.; Pillinger, M.; Santos, A. M.; Zhao, J.; Romão, C. C.; Gonçalves, I. S.; Kühn, F. E. *Eur. J. Inorg. Chem.* **2005**, 1716.

(38) Mukhamedova, L. A.; Kudryavtseva, M. I.; Shagidullin, R. R.; Samitov, Y. Y. *Russ. Chem. Bull.* **1973**, *22*, 1020.

(39) (a) Xia, Y.; Larock, R. C. *Green Chem.* **2010**, *12*, 1893. (b) Tan, S. G.; Chow, W. S. *Polym. Plast. Technol. Eng.* **2010**, *49*, 1581.